INTERMITTENT VERSUS FULLY-DEVELOPED BOILING IN A CLOSED TWO-PHASE THERMOSYPHON

A. Niro
Dipartimento di Energetica, Politecnico di Milano
Milano, Italy
and Dipartimento di Ingegneria Meccanica
Universita di Brescia
Brescia, Italy

P. A. Andreini and M Silvestri
Dipartimento di Energetica, Politecnico di Milano
Milano, Italy

G. P. Beretta
Dipartimento di Ingegneria Meccanica, Universita di Brescia
Brescia, Italy
and Department of Mechanical Engineering
Massachusetts Institute of Technology
Cambridge, Massachusetts

HTD-Vol. 104

VOLUME THREE

Buoyant Plumes in the Environment
Future Challenges in Environmental Heat Transfer
Measurements of Tissue Heat Transfer
Heat Transfer for Manufacturing in Space
General Papers

COLLECTED PAPERS IN HEAT TRANSFER 1988

presented at
THE WINTER ANNUAL MEETING OF
THE AMERICAN SOCIETY OF MECHANICAL ENGINEERS
CHICAGO, ILLINOIS
NOVEMBER 27-DECEMBER 2, 1988

sponsored by
THE HEAT TRANSFER DIVISION

edited by
K. T. YANG
UNIVERSITY OF NOTRE DAME

THE AMERICAN SOCIETY OF MECHANICAL ENGINEERS
United Engineering Center 345 East 47th Street New York, N.Y. 10017

INTERMITTENT VERSUS FULLY-DEVELOPED BOILING IN A CLOSED TWO-PHASE THERMOSYPHON

A. Niro
Dipartimento di Energetica, Politecnico di Milano
Milano, Italy
and Dipartimento di Ingegneria Meccanica
Universita di Brescia
Brescia, Italy

P. A. Andreini and M Silvestri
Dipartimento di Energetica, Politecnico di Milano
Milano, Italy

G. P. Beretta
Dipartimento di Ingegneria Meccanica, Universita di Brescia
Brescia, Italy
and Department of Mechanical Engineering
Massachusetts Institute of Technology
Cambridge, Massachusetts

Abstract

We present experimental results and theoretical considerations on the low-pressure boiling mechanisms in a closed two-phase thermosyphon and, in particular, on the transition between intermittent-boiling and fully-developed boiling.

We classify the boiling regimes on the basis of the frequency of bubble nucleation and the ratio of bubble diameter to device diameter. A criterion for the intermittent/fully-developed boiling frontier is based on the ratio of the bubble-nucleation waiting time and the bubble growth time. From this criterion we obtain a correlation between power throughput, working-fluid pressure and nucleation critical superheat. Experimental data on operating conditions, temperatures, and nucleation frequencies are in good agreement with the proposed correlation.

Nomenclature

a	liquid thermal diffusivity ($= K_f/\rho_f c_f$)
b	thermal boundary layer thickness
c_m	bubble growth constant (m=1 or 0.75)
c_f	liquid specific heat
c_3	coefficient of term grouping inertial and friction effects
D	device diameter
f	nucleation frequency ($=1/(\tau_w+\tau_g)$)
h_{fg}	vaporization hentalpy
Ja	Jakob adimensional number ($= \rho_f c_f \theta/\rho_g h_{fg}$)
k_f	liquid thermal conduttivity
p_f	liquid pressure
p_g	vapour pressure
$p_{g,ads}$	pressure of gas or vapour entraped in a cavity
Δp^*	critical pressure difference at bubble interface
q	thermal flux
R	bubble radius
R_s	contact area radius between bubble and surface
R_{d_1}	bubble radius at detachement for the static limit
R_{d_2}	bubble radius at detachement for the dynamic limit
T_g	vapour temperature
θ	liquid superheat
θ_w	liquid superheat at the wall
θ^*	critical superheat
ρ	density
σ	surface tension
τ_g	bubble growth time
τ_{g_1}	bubble growth time for the static limit
τ_{g_2}	bubble growth time for the dynamic limit
τ_w	nucleation waiting time
Φ	contact angle between bubble and heated surface

Introduction

The purpose of this work is to study experimentally and theoretically the boiling mechanisms in a closed two-phase thermosyphon for medium and large fillings, in order to define the frontiers between the main regimes and, in particular, the frontier between intermittent-boiling and fully-developed-boiling.

Closed two-phase thermosyphons (or wickless heat-pipes) can operate in two different ways depending on fluid filling: the "falling film evaporation" mode for little fillings (liquid volume less than about 10% of the evaporator volume), and "pool boiling" for medium and large fillings (from 30% to100% and over). In the falling-film evaporation mode all the thermosyphon walls are wetted by a continuous liquid film which, however, for most fluids is stable only at very low thermal fluxes. In the pool-boiling mode, instead, the thermosyphon evaporator is flooded, boiling is sustained over a wide range of operating fluids and conditions, and the power throughput is much greater. Therefore, pool-boiling is the mode of operation of technological interest. However, there are many boiling regimes characterized by different degrees of steadiness,

which affect differently the thermosyphon performance.

In the last fifteen years the fluid dynamic phenomena related to mass, momentum and heat transfer between evaporator and condenser have been extensively studied in order to determine the operating limits; Imura et a. (1983) reviewed about ten different relations for the flooding limit. The boiling phenomena in the evaporator have been almost always overlooked, even in some new theoretical models (Dobran, 1985; Reed and Tien, 1987), although instabilities and unsteady regimes have been known for a long time (Larkin, 1971; Bezrodnyi et a., 1977) to depend on the details of the boiling mechanisms. Casarosa and Latrofa (1983) have clearly shown experimentally the existence of also strongly intermittent boiling regimes.

To optimize the performance of a closed two-phase thermosyphon, the designer must avoid such regimes and, therefore, be aware of the causes of the unsteady behavior. Unsteady regimes cause large-amplitude oscillations in many characteristic variables, such as the evaporator wall temperature that can exceed the design values. Moreover, for evaporator fixed-temperature boundary conditions, the operation may result blocked when not expected. However, no correlations for the frontier between the intermittent-boiling and the fully-developed-boling regimes are available in the literature.

In this paper, we first review the boiling regimes and the causes of unsteady operation; then, we propose criteria for classifying the main regimes and obtain an analitical correlation for the intermittent-boiling /fully-developed-boiling frontier; finally, we discuss the experimental results and a diagram where the frontiers are plotted.

Boiling Regimes

If the thermosyphon is initially isolated, the liquid is at rest in the evaporator and is in thermodynamic equilibrium with its vapour that fills the remaining volume of the device. The temperature is imposed by the heat sink, in contact with the thermosyphon through the condenser. At time t_0 we begin to power the heat source, the liquid starts to superheat. Evaporation begins from the free surface. Boiling, instead, starts when the liquid reaches a critical superheat, i.e., a critical value of temperature greater than the saturation temperature corresponding to the pressure in the device. The critical superheat for bubble nucleation depends on the heated surface characteristics (roughness, adsorbed gases or vapours) and the thermodynamic properties of the fluid (vapour density and enthalpy of vaporization).

Depending on the extent of the critical liquid superheat, boiling may be characterized by quite a wide spectrum of nucleation frequencies and bubble dimensions. The nucleation frequencies can range from less than 0.01 Hz to more than 50 Hz. Clearly, the lower is the nucleation frequency, the more uneven and unsteady becomes the operation of a closed two-phase thermosyphon. Low nucleation frequencies (less than 0.1 Hz) are related to high liquid superheats that cause the formation of large bubbles (with respect to the device diameter). Thus long periods of liquid quietness (up to several hundreds of seconds) alternate with sudden and almost explosive vapour nucleations. The nucleation is generally followed by strong boiling that quickly goes out giving way to a new period of quietness. High nucleation frequencies (higher than 10 Hz) bring about the fully-developed boiling regime: thick jets of small bubbles (1-2 mm diameter) detach from one or more active cavities on the heated surface, making strongly turbulent the fluid in the evaporator. For frequencies between 0.1 Hz and 10 Hz we have transition regimes characterized by intermediate bubble growth rates and bubble dimensions. According to these observations, we classify the different regimes based on the nucleation frequency and the ratio of bubble diameter to device diameter.

The boiling process consists of the sequence of the processes of bubble nucleation, growth and detachment. Experimentally we observe that nucleation in our thermosyphons always occurs on the wall. This is because the heated surface has a some roughness -- cavities and scratches of various size that become active if some gas or vapour is entrapped. Nucleation occurs at an active cavity when the liquid reaches the critical superheat

$$\theta^* \approx \frac{1}{dp_s/dT}\,\Delta p^* = \frac{1}{dp_s/dT}\left(\frac{2\sigma}{R_c} - p_{g,ads}\right) \qquad (1)$$

where Δp^* is the difference between vapour pressure and liquid pressure when the nucleus reaches the critical dimensions (we assume a hemispherical critical nucleus with a radius equal to the mouth cavity radius R_c as suggested by Griffith and Wallis, 1965) and $p_{g,ads}$ is the pressure of the gas or vapour entrained in the cavity. Relation 1 is valid for the case of uniform liquid superheat. Since this hypothesis is not actually verified, we further assume (as suggested by Hsu, 1962) that the critical superheat θ^* is reached by a liquid layer of thickness b near the heated wall. For b we assume the value 1.5 R_c proposed by Han and Griffith, 1965. From Relation 1 we see that, for a given roughness and adsorbed gas or vapour, the lower is dp_s/dT the higher is the critical superheat. For example, for water dp_s/dT decreases by a factor of 50 between 120 and 20°C and, therefore, the superheats needed for nucleation at 20°C are 50 times higher than at 120 °C.

We define the waiting time τ_w as the time needed to attain the critical superheat θ^* in the layer of thickness b. The waiting time ends and the growth time τ_g begins when the vapour nucleus, after reaching the critical dimension, starts to grow quickly. The growth time ends when the bubble detaches from the heated surface. The inverse of the period of a whole cycle, i.e., of the sum of the waiting time and the growth time is defined (Han and Griffith, 1965) as the nucleation frequency

$$f = \frac{1}{\tau_w + \tau_g} \qquad (2)$$

For τ_w much longer than τ_g, the nucleation frequency obviously coincides with the inverse of the waiting time.

Intermittent vs Fully-Developed Boiling Frontier

We say that boiling is "fully developed" when the waiting time τ_w is much shorter than the growth time τ_g, whereas boiling is "intermittent" when the waiting time τ_w is much longer than the growth time τ_g. Thus, the transition frontier between the intermittent boiling regime and the fully developed boiling regime is determined by the criterion

$$\tau_w \sim \tau_g \tag{3}$$

In order to derive from Criterion 3 a relation between fluid thermodynamic properties, geometric characteristics and system boundary conditions, we need to estimate τ_w and τ_g.

Determination of τ_w. The waiting time τ_w can be determined by the general nucleation criterion

$$\theta(R-b,z_s,\tau_w) = \theta^* \tag{4}$$

where $\theta(r,z,t)$ is the relation describing in cilindrical coordinates the liquid superheat as a function of the distance r from the evaporator axis, the height z_s in the evaporator of the nucleation site, and time t. The liquid superheat near the heated surface is determined by three contributions: (a) the thermal boundary layer; (b) the bulk heating of the liquid in the evaporator; and (c) the cooling of the vapor in the condenser which reduces the vapor temperature and, hence, the saturation pressure and temperature. However, the characteristic times of the three superheat mechanisms are quite different: the boudary-layer characteristic time is in the order of 0.1 s and is much shorter than the characteristic times of the other two mechanisms (Niro, 1987) which are of the order of 10 s. Since the bubble growth time τ_g is always shorter than 200 ms and the waiting time τ_w at the transition frontier is of the same order of magnitude of τ_w (Criterion 3), we can consider only the thermal boundary layer contribution θ_w and neglect the other two mechanisms. If we express θ_w more conveniently in cartesian coordinates, i.e., $\theta_w=\theta_w(x,z,t)$ where x is the distance from the heated wall, and further assume that it depends weakly on height z, Relation 4 becomes

$$\theta_w(b,\tau_w) = \theta^* \tag{5}$$

Assuming a purely conductive heat transfer mechanism in the liquid near to the heated wall, the waiting time may be approximated by the relation

$$\tau_w = \frac{\pi}{4}\left(1 + \frac{bq}{k_f\theta^*}\right)^2 k_f \rho_f c_f \frac{\theta^{*2}}{q^2} \tag{6}$$

obtained by linearizing the conductive solution for semi-infinite geometry and fixed thermal flux boundary conditions.

Determination of τ_g. To determine the growth time we need the bubble growth law and the force balance that controls bubble detachment from the heated surface. At the detachment instant, the force balance is

$$F_b = F_s + F_{Ii} + F_f \tag{7}$$

i.e., buoyancy (F_b) balances surface adhesion forces (F_s), liquid inertia (F_{Ii}) and viscous drag (F_f). We observed experimentally (by a high speed camera) that the shape of the growing bubble is nearly spherical (also for high superheat). Thus, the Balance 7 may be written as

$$\frac{4}{3}\pi R^3 \rho_f g = 2\pi\sigma R_s \sin\Phi + \frac{4}{3}\pi R^2\dot{R}^2\rho_f + \frac{c_w}{2}\pi R^2\dot{R}^2\rho_f \tag{8}$$

where R_s is the contact radius between bubble and surface (assumed to be constant and independent of the bubble radius R). $\dot{R}$ is the bubble detachment velocity (the bubble is assumed to be tangent to the heated surface), c_w is an empirical coefficient, as the friction forces are not sufficiently known. The angle Φ would be the contact angle between bubble and heated surface for a horizontal surface. Here we assume that Φ includes also a geometric factor, taking into account that our surface is vertical. The inertial term is derived from the Witze (1968) solution, obtained for a spherical bubble growing tangent to the surface in semiinfinite liquid and for inviscid and irrotational flow. The assumption of semiinfinite liquid implies that Balance 8 holds only for small bubbles with respect to the device diameter. This assumption is further discussed later. Since inertial forces and viscous forces have the same functional dependence from R and $\dot{R}$, they may be grouped in a single term $c_3\pi R^2\dot{R}^2\rho_l$.

Determining the bubble growth law as a function of liquid superheat and thermodynamic properties is a hard problem. For small superheats and a pressure not much lower than atmospheric, the growth is wholly controlled by the heat transfer mechanisms (negligible liquid inertia) we find the so-called 'asymptotic solution'

$$R = c_1\, Ja\sqrt{at} \tag{9'}$$

Where Ja is Jakob's dimensionless number, $Ja=(\rho_f c_f \theta/\rho_g h_{fg})$, and a the liquid diffusivity, $a= K_f/\rho_f c_f$. Appendix A discusses the range of validity of Equation 9'.

When the inertial effects are not negligible, Equation 9' ceases to hold and the bubble growth law becomes complex (Mikic et a., 1970; Van Stralen et a., 1975; Zijl et a. 1979). Since we need an analytical expression, we use the empirical growth relation proposed by Cole and Shulman (1966):

$$R = c_{0.75}\, Ja^{0.75}\sqrt{at} \tag{9"}$$

Appendix A discusses the range of validity also for Equation 9". Both Equations 9' and 9" can be written in the form

$$R = c_m Ja^m \sqrt{at} \qquad (10)$$

Using Equation 10 in Balance 8, we obtain the growth time

$$\tau_g = \left(c_m c_3 \left(\frac{a}{g^2}\right)^{1/2} Ja^m + \frac{3\sigma R_s \sin\Phi}{2\varrho_f g c_m^3 Ja^{3m} a^{1.5}} \right)^{2/3} \qquad (11)$$

The first term within brackets is the ratio between dynamical forces (liquid inertia and viscous drag) and buoyancy; the second term is the ratio between surface adhesion force and buoyancy. Relation 11 has two interesting limit solutions

$$\tau_{g_1} = \left(\frac{3\sigma R_s \sin\Phi}{2\varrho_f g}\right)^{2/3} \frac{1}{c_m^2 Ja^{2m} a} \qquad (12)$$

$$\tau_{g_2} = (c_m c_3)^{2/3} \left(\frac{a}{g^2}\right)^{1/3} Ja^{(2/3)m} \qquad (13)$$

Equation 12, that we call the static solution, holds when adhesion forces prevail over liquid inertia, i.e., when

$$c_m c_3 Ja^m \left(\frac{a}{g^2}\right)^{1/2} << \frac{3\sigma R_s \sin\Phi}{2\varrho_f g c_m^3 Ja^{3m} a^{1.5}}$$

or, equivalently,

$$Ja << \left(\frac{3\sigma R_s \sin\Phi}{2c_3 \varrho_f g c_m^4} \frac{a}{g^2}\right)^{1/4m} = \tilde{Ja} \qquad (14')$$

Equation 13, that we call the dynamic solution, holds when liquid inertia prevails over adhesion forces, i.e., when

$$Ja >> \tilde{Ja} \qquad (14")$$

Intermittent/Fully-Developed Boiling Frontier Relation. Substituting Relations 6 and 11 in Criterion 3, and assuming that the term $(bq/k_f\theta^*)$ in the Relation 6 is negligible, we find the relation

$$q \geq \frac{\sqrt{\pi k_f \varrho_f c_f}}{2} \frac{\theta}{\left(c_m c_3 \left(\frac{a}{g^2}\right)^{1/2} Ja^m + \frac{3\sigma R_s \sin\Phi}{2\varrho_f g c_m^3 Ja^{3m} a^{1.5}} \right)^{1/3}} \qquad (15)$$

that describes the transition frontier between intermittent boiling and fully developed boiling.

In the dynamic limit ($Ja >> \tilde{Ja}$) and the static limit ($Ja << \tilde{Ja}$), Relation 15 can be simplified, respectively, to yield

$$q \geq \frac{\sqrt{\pi}}{2(c_{0.75} c_3)^{1/3}} (g k_f)^{1/3} (\varrho_f c_f)^{5/12} \frac{\Delta p^{0.75} T^{0.25}}{\sqrt{p'}} \qquad (16)$$

$$q \geq \frac{\sqrt{\pi}}{2} c_{0.75} k_f \varrho_f c_f \left(\frac{2\varrho_f g}{3\sigma R_s \sin\Phi}\right) \frac{\Delta p^{0.75}}{p'^3 T} \qquad (17)$$

where p' denotes dp_s/dT. Relations 16 and 17 are obtained using, respectively, Relations 9" and 9', and replacing in the Jakob number Relation 1 and the Clausius-Clapeyron equation, i.e., the relation

$$Ja = \frac{\varrho_f c_f}{\varrho_g h_{fg}} \theta = \frac{\varrho_f c_f}{p'^2 T} \Delta p \qquad (18)$$

It is interesting to point out that the functional dependence of the thermal flux q from the superheat $\theta \sim 1/p'$ ranges from $q \sim \theta^{0.5}$ to $q \sim \theta^3$ depending on whether the bubble growth is dominated by dynamic forces or static forces. If dynamic forces dominate, bubbles are not frequent and not small enough to yield fully-developed boiling; thus the functional dependence between q and θ is not what we have in boiling.

Criteria For The Other Frontiers

The regimes are characterized not only by the nucleation frequency $f=1/(\tau_w+\tau_g)$, but also by the bubble dimensions with respect to the device diameter. For the same nucleation frequency we may have different regimes depending on the device diameter, according to the three criteria

$$D_d/D << 1, \quad D_d/D >> 1, \quad D_d/D \sim 1 \qquad (19)$$

Substituting Equations 11, 12 and 13 in the growth law Equation 10, we get the bubble radius at detachment, respectively, for the general case and the two limit solutions (static and dynamic), i.e.,

$$R_d = \left(c_m c_3^4 \left(\frac{a^2}{g}\right) Ja^{4m} + \frac{3\sigma R_s \sin\Phi}{2\varrho_f g} \right)^{1/3} \qquad (20)$$

$$R_{d_1} = \left(\frac{3\sigma R_s \sin\Phi}{2\varrho_f g}\right)^{1/3} \qquad Ja << \tilde{Ja} \qquad (20')$$

$$R_{d_2} = c_m^{1/3} c_3^{4/3} \left(\frac{a}{g^2}\right)^{1/3} Ja^{(4/3)m} \qquad Ja >> \tilde{Ja} \qquad (20")$$

For $R_s = R_{d_1} \sin\Phi$, Relation 20' becomes the known Fritz-Hende relation.

If Relations 20 and 18 are put in Criteria 19, we obtain three interesting conditions. Criterion $D_d/D<<1$ identifies bubbles that are very small and corresponds to the fully-developed boiling regime. Criterion $D_d/D>>1$ identifies very large bubbles and corresponds to a low-frequency boiling regime. Criterion $D_d/D\sim1$ identifies bubbles with dimensions that are comparable with the device diameter, and corresponds to a slug flow regime. Clearly, the use of Relation 20 in the criteria $D_d/D>>1$ and $D_d/D\sim1$ would yields

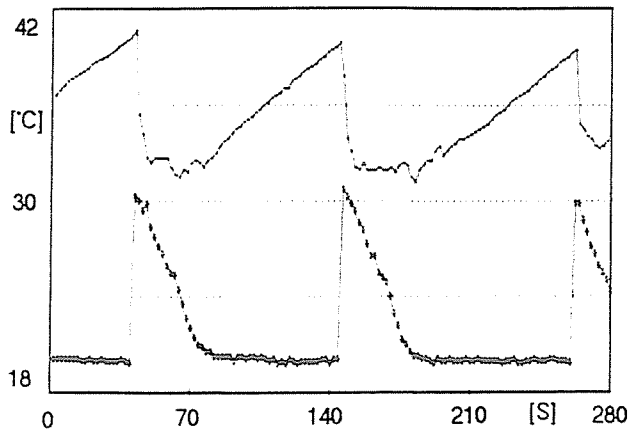

Fig. 1 Liquid and vapour temperature in a low-frequency boiling regime. (D= 12 mm, water, $P_r = 10^{-4}$ and Q= 13 W)

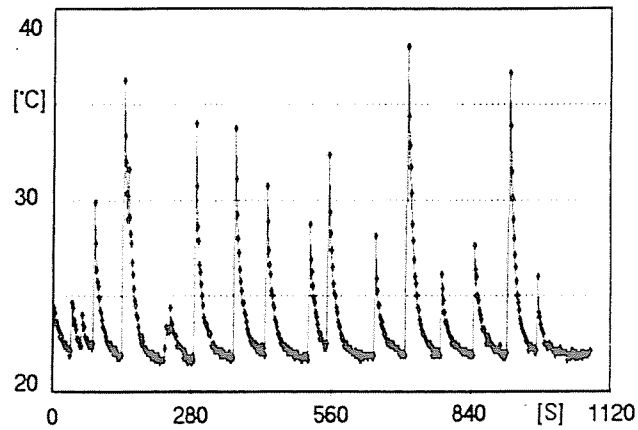

Fig. 2 Liquid and vapour temperature in a low-frequency boiling regime. (D= 12 mm, water, $P_r = 10^{-4}$ and Q= 32 W)

only qualitative results because Relation 20 implies the assumption $D_d/D \ll 1$.

Experimental Results

The experimental study is aimed to gather information about the boiling regimes and the transition frontier between intermittent boiling and fully-developed boiling. To this end, we studied the trend of nucleation frequencies as a function of pressure and power throughput.

The experimental results are obtained with a specifically designed facility equipped with transparent pipes of 12 and 30 mm internal diameter and 1000 mm length. Evaporator, adiabatic section and condenser are respectively 300 mm, 400 mm and 400 mm length. The evaporator is electrically heated by a Nichel-Chrome ribbon externally wound around it. Liquid and vapour temperatures are measured by thermocouples directly exposed to the fluid and placed respectively at 50 mm from the evaporator bottom and 300 from the condenser top. The input and output power and the fluid pressure are also measured. Errors on temperature measurements are less than 0.1°C. Errors on measurements of input power, output power and pressure are respectively 15%, 5% and 0.5%. The relatively high error on the input power measurement is due to the lack of thermal insulation around the evaporator. All measures are sampled automatically by an on-line computer at a maximum rate of 10 Hz. A video-recording of the thermosyphon operation is also performed by a video-camera and a stroboscope (the camera recording frequency is 50 Hz, but each frame is exposed for only10 μs).

The thermosyphons are operated vertically. Most tests are run with water as the working fluid, some are run with acetone. The liquid filling corresponds to 80% of evaporator volume. To span the transition between intermittent and fully-developed boiling, the operating conditions are varied so that the fluid pressure, expressed as reduced pressure, ranges between 10^{-4} and 10^{-2}. The tests are grouped in sequences carried out by changing the power throughput while holding the pressure at a fixed constant value different for every sequence.

A typical trend of liquid temperature (higher graph) and vapour temperature (lower graph) in a low-frequency boiling regime (about 0.01 Hz) is shown in Figure 1, where the waiting phase and the boiling phase can be clearly recognized. During the waiting phase, evaporator and condenser are weakly coupled. The liquid at rest in the evaporator is superheating, and the vapour in the condenser is cooling. The liquid temperature at the bottom of the evaporator rises almost linearly, whereas the vapour temperature in the condenser falls almost exponentially, as shown by Figure 2, with a measured characteristic time of about10 s, approaching the condenser wall temperature. When the critical superheat is achieved, vapour nucleation occurs. Due to the high available superheat, the bubble growth rate and its dimensions are so large that the liquid above the nucleation site is suddenly and violently ejected into the condenser. This causes a sharp rise of the condenser temperature. The final vapour temperature is lower than the measured liquid temperature because this is measured at the bottom of the evaporator where it is higher due to stratification built up during the waiting time. After the first burst, nucleation continues with decreasing intensity, stimulated by pressure perturbations. The liquid temperature decreases due to the mixing of liquid remained in the evaporator with the cooled liquid returning from the condenser. As the pressure perturbations weaken, boiling dies out and a new waiting phase begins. The dynamically controlled nucleation, in fact, unlike thermally controlled nucleation is not stable. The pressure in the thermosyphon remains always very close to the saturation pressure corresponding to the temperature of the vapor.

As the power throughput is increased, the critical superheat is attained in a shorter time and the waiting time between two successive bursts decreases, i.e., the burst frequency increases. As the burst frequency increases, nonlinear phenomena such as pressure perturbations appear. These phenomena favour the nucleation and cooperate to further increasing the average nucleation frequency, as shown in Figure 3. The trend of liquid and vapour temperatures in fully-developed boiling is shown in Figure 4. The temperatures still experience fluctuations,

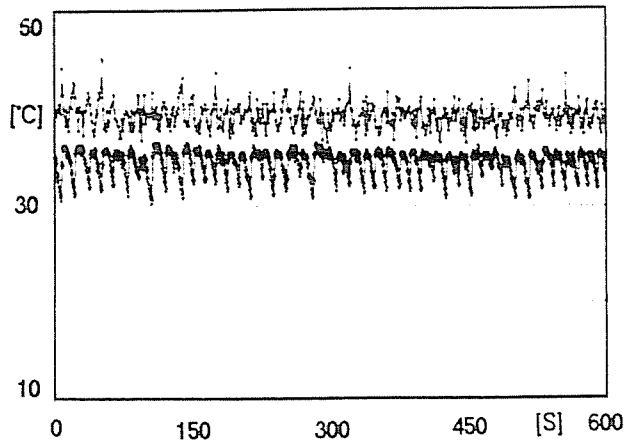

Fig. 3 Liquid and vapour temperature in a intermediate-frequency boiling regime. (D=12 mm, water, $P_r = 10^{-4}$ and Q= 176 W)

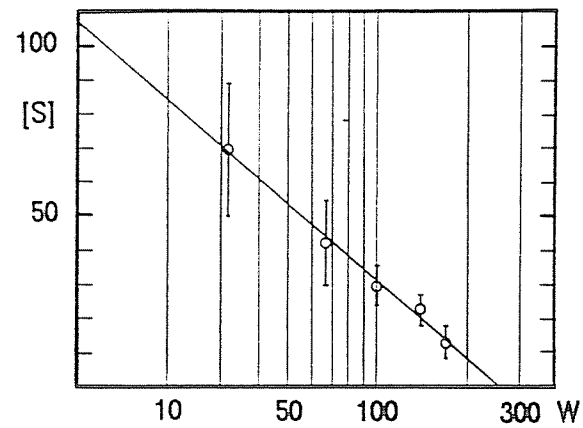

Fig. 5 Dependence of the average waiting time on power throughput. (D= 12 mm, water, $P_r = 10^{-4}$, Q(0)= 250 W; r=0.996)

but these are restrained in 0.5 °C for the liquid and 0.8 °C for the vapour. These fluctuations, which remain also at high nucleation frequencies, are due to the intrinsically unsteady nature of boiling.

The thermosyphon operation is steady only "on average", i.e., for a given pressure and power throughput, we do not have a single nucleation frequency, but a spectrum of frequencies which are related to phenomena such as stimulated nucleation and random operation decoupling. Thus, for each test we need to recognize a charateristic nucleation frequency. We conjecture that information about nucleation frequencies may be inferred by a spectral analysis of liquid or vapour temperatures. In this respect, we note that the vapour conditions are much more uniform than the liquid conditions and thus the vapor temperature is more suitable for this kind of analysis.

The estimate of the longer waiting times ($\tau_w \geq 10$ s), such as for the traces in Figure 2, is done as follows. The waiting period starts when the measured vapor temperature begins to fall exponentially, i.e., when the evaporator and the condenser decouple. The waiting period ends when the vapor temperature, after falling below a low-threshold value predetermined for each run on the basis of a visual and a statistical analysis of the traces, has a jump greater

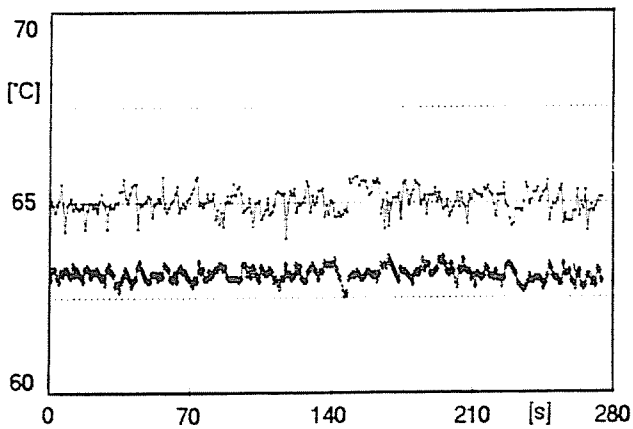

Fig. 4 Liquid and vapour temperature in fully-developed boiling regime. (D= 12 mm, water, $P_r = 10^{-4}$ and Q= 36 W)

than a threshold amplitude. When this occurs, a boiling burst couples again the condenser to the evaporator. The low-threshold temperature is chosen as the temperature below which the vapor stays for 67% of the test time. To estimate the shorter waiting times ($\tau_w < 10$ s but greater than or equal to 0.5 s that is the minimum significative time interval consistent with our sampling rate), such as for the traces in Figure 3, only temperature oscillations of amplitude smaller than a threshold amplitude are considered, i.e., we do not consider the longer random operation decouplings. For each test, we determine the average value and the variance of the waiting time. Elimination-inclusion procedures have been also performed in order to minimize the variance.

Figure 5 shows the dependence of the average waiting times τ_w on power throughput Q in a semilogarithmic scale; the graph refers to a given value of the pressure. Extrapolation of these data to zero waiting time yields a value of power throughput that we take as indicative of the minimum power needed at the given pressure for the onset of fully-developed boiling . The values of power throughput determined in this way are given in Table 1. The data show a strong dependence on $1/\sqrt{p'}$, specifically, the same functional dependence as our Equation 16 for the intermittent/fully-developed boiling frontier in the dynamic limit. Assuming that Δp^* is constant for all runs and that the variations of properties ϱ_f, c_f, k_f with temperature are negligible between 20 and 80°C, then Equation 16 may be written as

$$q \geq G \frac{T^{0.25}}{\sqrt{p'}} \qquad (21)$$

As shown in Figure 6, the experimental data correlate linearly with $T^{0.25}/\sqrt{p'}$ with a correlation coefficient of 0.976 and a scatter of about 25%. For the constant G we find the value of G = 89670 (all variables in SI units). The assumption that Δp^* is constant is reasonable because all runs are performed on devices with the same surface roughness and the same clearness degree, but it could not be checked experimentally. Using the values given in Ap-

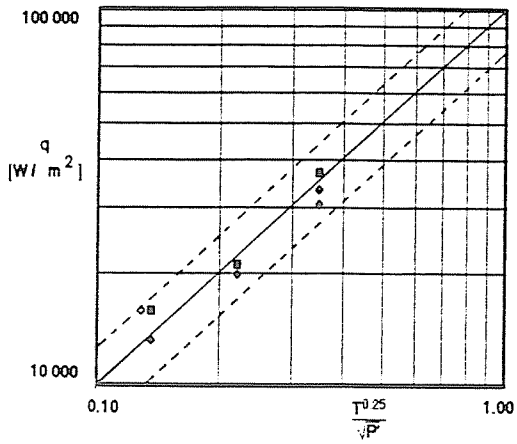

Fig. 6 Correlation for intermittent/fully-developed boiling frontier.
◆ D12, water; ■ D30, water; ◇ D12, Acetone

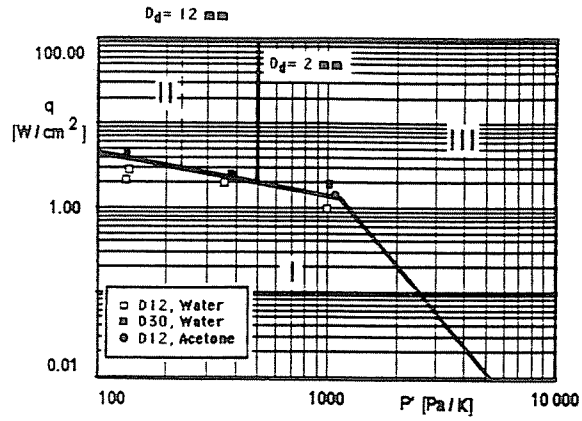

Fig. 7 Frontiers between the main boiling regimes
(I) Intermittent boiling
(II) Developed boiling with slug regime
(III) Fully-developed boiling

pendix A for the constants $c_{0.75}$ e c_3, we get $\Delta p^* = 670$ Pa from the constant G. Using this value we estimate the Jakob numbers given in Table 1.

Figure 7 shows the experimental data and Relations16 and 17 on a p'-q diagram. The two relations refer to the transition frontier in the dynamic and the static limit, respectively. The intersection point of these two limit solutions occurs for $Ja = \widetilde{Ja} \approx 30$ (for water). At that point the power is overestimated by only17% compared to that given by the complete solution (Relation 15). Thus, the two limit solutions give a good approximation of the frontier between the intermittent and fully-developed boiling regimes.

The criteria $D_d << D$ and $D_d \simeq D$, are also plotted in Figure 7. The values for these two curves are obtained by substituting Relations 15 and 18 in the criteria. The location of the $D_d \simeq D$ boundary (dotted line) is only qualitative because it is obviously inconsistent with the assumption $D_d << D$ used in deriving the relation for the detachment diameter D_d.

P_r	T (°C)	T (K)	$\frac{d\rho}{dT}$ (SI)	Ja (*)	Q (W)	q (W/m²)	$\frac{T^{0.25}}{\sqrt{P'}}$ (SI)	Notes
10^{-4}	19	292	138	508	250	$3.316 \cdot 10^4$	0.351	D12-H_2O
10^{-4}	19	292	138	508	230	$3.050 \cdot 10^4$	0.351	D12-H_2O
10^{-4}	19	292	138	508	700	$3.714 \cdot 10^4$	0.351	D30-H_2O
$3 \cdot 10^{-4}$	38	311	359	70	150	$1.989 \cdot 10^4$	0.221	D12-H_2O
$3 \cdot 10^{-4}$	38	311	359	70	400	$2.122 \cdot 10^4$	0.221	D30-H_2O
10^{-3}	62	335	995	8	100	$1.326 \cdot 10^4$	0.136	D12-H_2O
10^{-3}	62	335	995	8	700	$1.592 \cdot 10^4$	0.136	D30-H_2O
$5 \cdot 10^{-3}$	20	293	1033	4	120	$1.544 \cdot 10^4$	0.129	D12 Acetone

(*) The Jakob numbers are estimated using the value ΔP=670 Pa.

Tab.1 Data on intermittent/fully-developed boiling frontier

In summary, three regions are defined in the p'-q plane. In Region I we have intermittent boiling (the farther we operate from the frontier the lower is the nucleation frequency). In region II we have developed boiling, but the bubbles have dimensions comparable to the device dimension (slug regime). In region III we have fully-developed boiling, characterized by thick jets of small bubbles. Of course, the three regions are bounded in the upper part by a fourth region, not plotted, where the thermosyphon cannot operate due to the onset of some critical condition or operating limit. It is noteworthy that the p'-q plane is perfectly equivalent to a p-q or p_r-q plane, since the saturation pressure is a monotone and convex function of temperature. Here, we have chosen the variable p' rather than p so as to avoid empirical or numerical relations in Equations 16 and 17.

Conclusions

Especially at low-pressures, the performance of a closed two-phase thermosyphon with medium and large filling, is characterized by unsteady operation. Our analysis and experimental data show that the reason for such unsteady operation is to be found in the boiling mechanisms. Boiling may occur with a wide spectrum of different nucleation frequencies and bubble dimensions depending on liquid superheat, vapor density and other thermodynamic properties.

We classify the boiling regimes on the basis of the frequency of bubble nucleation and the ratio of bubble diameter to device diameter. A criterion for the intermittent/fully-developed boiling frontier is based on the ratio of the bubble-nucleation waiting time and the bubble growth time. From this criterion we obtain a correlation between power throughput, working-fluid pressure and nucleation critical superheat (Relations 16 and 21). This correlation explains the known empirical observation that intermittent boiling regimes are related to low operating pressures.

An experimental analysis performed on transparent devices using mainly water as the working fluid yields the dependence of nucleation frequencies on power throughput

and operating pressure. The data are in good agreement with the proposed relation (in the dynamic limit, Equation16) for the frontier between the intermittent-boiling and fully-developed-boiling regimes. More data spanning a broader range of operating conditions and, perhaps, including measurement of local superheat, are needed to further validate our theoretical considerations. Also, data on bubble growth in constrained geometries are needed in order to better determine the bubble dimensions at detachment and extend the validity of our results. Finally, work is needed to evaluate the usefulness of power spectrum analyses and phase-plane analyses to better characterize the bubble nucleation frequency.

References

Bezrodnyi, M. K., and Elekseyenko, D. Y., 1977, "Boiling heat transfer in a closed two-phase thermosyphon", *HEAT TRANSFER-Soviet Research*, vol. 9, pp.14-20.

Casarosa, C., and Latrofa, E., and Shelginski, A., 1983, "The geyser effect in a two-phase closed thermosyphon", *Int. J. Heat Mass Transfer*, vol. 26, pp. 933-941.

Cole, R., and Shulman, H. L., 1966, "Bubble growth at high Jakob numbers", *Int. J. Heat Mass Transfer* vol. 9, pp. 1377-1390.

Dobran, F., 1985, "Steady-state characteristics and stability thresholds of a closed two-phase thermosyphon", *Int. J. Heat Mass Transfer*, vol. 28, pp. 949-957.

Griffith, P., and Wallis, J. D., 1960, "The role of surface conditions in nucleate boiling", *Ch. Eng. Progr., Symp. Ser*, vol. 56, p. 49.

Han, C. Y., and Griffith, P., 1965, "The mechanism of heat transfer in nucleate pool boiling - Part I: bubble initiation, growth and departure", *Int. J. Heat Mass Transfer*, vol. 8, pp. 887-904.

Hsu, Y. Y., 1962, "On the size range of the active nucleation cavities on a heating surface", *ASME J. Heat Transfer*, vol. 84, p. 207.

Imura, H., Sasaguchi, and Kozai, H., 1983, "Critical heat flux in a closed two-phase thermosyphon", *Int. J. Heat Mass Transfer*, vol. 26, p. 1181.

Kiper, A. M., 1971, "Minimum bubble departure diameter in nucleate pool boiling", *Int. J. Heat Mass Transfer*, vol. 14, pp.931-937.

Larkin, B. S., 1971, "An experimental study of two-phase thermosyphon tube", *Trans. Can. Soc. Mech. Eng.*, vol.14, p.17.

Mikic, B. B., Rohsenow, W. M., and Griffith, P., 1970, "On bubble growth rates", *Int. J. Heat Mass Transfer*, vol.13, pp.657-666.

Niro, A., 1987, "Study of closed two-phase thermosyphon", Ph.D Thesis, Politecnico di Milano, Milano, Italy.

Reed, J. G., and Tien, C. L., 1987, "Modeling of the two phase closed thermosyphon", *ASME J. Heat Transfer*, vol. 109, p. 722.

Stewart, J. K., and Cole, R., 1972, "Bubble growth rates during nucleate boiling at high Jakob numbers", *Int. J. Heat Mass Transfer*, vol. 15, pp. 655-663.

Yan Stralen, S. J. D., Cole, R., Sluyter, W. M., Sohal, M. S., 1975a, "Bubble growth rates in nucleate boiling of water at subatmosperic pressures", *Int. J. Heat Mass Transfer*, vol. 18, pp. 655-669.

Yan Stralen, S. J. D., Sohal, M. S., Cole, R., and Sluyter, W. M., 1975b, "Bubble growth rate in pure and binary systems: combined effect of relaxation and evaporation microlayers", *Int. J. Heat Mass Transfer*, vol. 18, pp. 453-467.

Witze, C. P., Schrock, Y. E., and Chambré, P. L., 1968, "Flow about a growing sphere in contact with a plane surface", *Int. J. Heat Mass Transfer*, vol. 11, pp. 1637-1652.

Zijl, W., Ramakers, F. J. M., and Yan Stralen, S. J. D., 1979, "Global numerical solutions of growth and departure of a vapour bubble at a horizontal superheated wall in a pure liquid and a binary mixture", *Int. J. Heat Mass Transfer*, vol. 22, pp. 401-420.

Appendix A

During bubble growth, the vapor pressure is related to the motion of the liquid-vapor interface and the mass and energy flux through it. For a spherical bubble growing on a surface in a uniformly superheated liquid at temperature T_{f_∞} and pressure p_f, the momentum and energy equations are

$$2(R\ddot{R}+\dot{R}^2)\ln\left(\frac{R}{R_0}\right)\cos\frac{\phi}{2}+2\dot{R}^2\cos^2\frac{\phi}{2}=\frac{p_g-p_f}{\varrho_f}-\frac{2\sigma}{\varrho_f R} \qquad (A.1)$$

$$T_{f_\infty}-T_g=\frac{\varrho_g h_{fg}}{k_l}\sqrt{\pi a t}\,\dot{R} \qquad (A.2)$$

Equation A.1 is that derived by Witze (1968) for inviscid and irrotational flow. Unlike the case of bubble growth in infinite geometry, the vapor pressure depends on the angle at center ϕ and has a maximum at bubble top (ϕ=0). The vapor, for its high diffusivity, may be assumed to be at saturation conditions, i.e., $p_g \equiv p_s(T_g)$. Assuming

$$2\sigma/p_f R \ll 1 \qquad (A.3)$$

the right hand side of Eqation A.1 becomes

$$RHS=\frac{p_g-p_f}{\varrho_f}=$$

$$=\frac{1}{\varrho_f}[p_s(T_{f_\infty})-p_f]\left(1-\frac{p_s(T_{f_\infty})-p_g}{p_s(T_{f_\infty})-p_f}\right)=\frac{\Delta p^*}{\varrho_f}\left(1-\frac{T_{f_\infty}-T_g}{T_{f_\infty}-T_s(p_f)}\right)$$

Moreover, neglecting the inertial terms, i.e., assuming

$$\frac{2(R\ddot{R}+\dot{R}^2)\ln(R/R_0)\cos(\phi/2)+2\dot{R}^2\cos^2(\phi/2)}{\Delta p^*/\varrho_f}\ll 1 \qquad (A.4)$$

Equation A.1 becomes

$$\frac{T_{f_\infty}-T_g}{T_{f_\infty}-T_s(p_f)}\approx 1 \qquad (A.1')$$

Thus, bubble growth is controlled only by the energy equation, i.e.,

$$T_{f_\infty}-T_s(p_f)=\frac{\varrho_g h_{fg}}{k_l}\sqrt{\pi a t}\,\dot{R} \qquad (A.2')$$

which yields Equation 9' where is $\theta = T_{f_\infty}-T_s(p_f)$. Using Equation 9', Conditions A.3 and A.4 become

$$\frac{2\sigma}{p_f\, c\mathrm{Ja}\sqrt{at}}\equiv\frac{2\sigma}{p_f\, c\mathrm{Ja}\sqrt{a\tau_g}\,\sqrt{(t/\tau_g)}}\ll 1 \qquad (A.3')$$

$$\frac{c^2\mathrm{Ja}^2(a/t)}{\Delta p^*/\varrho_f}\equiv\frac{c^2\mathrm{Ja}^2(a/\tau_g)}{(t/\tau_g)\ \Delta p^*/\varrho_f}\ll 1 \qquad (A.4')$$

Assuming that Conditions A.3' and A.4' hold at the beginning of bubble growth, i.e., for $t \ll \tau_g$, and using Relation 12 for τ_g we obtain

$$p_f \gg \frac{2\sigma}{\frac{t}{\tau_g}\left(\frac{3\sigma R_s\sin\Phi}{2\varrho_f g}\right)^{1/3}}\approx 600\ \mathrm{Pa} \qquad (A.3'')$$

$$\mathrm{Ja}\ll\left(\frac{1}{c^2 g^2}\left(\frac{3\sigma R_s\sin\Phi}{2\varrho_f g}\right)^{2/3}\frac{\Delta p^*}{\varrho_f}\frac{t}{\tau_g}\right)^{1/4}\approx 60 \qquad (A.4'')$$

Condition (A.3") is satisfied in most situations. Thus, Condition (A.4") implies that the "diffusive" solution (Relation 9') is valid for Ja ≤10. A large collection of data taken from the literature (Kiper, 1971; Stewart and Cole, 1972; Yan Stralen et a., 1975b) show good agreement with the empirical solution (9") for Ja ≥ 20 provided we take $c_{0.75}$ = 2. The constant c_3 may be obtained by a best fit of Relation 20 on the same experimental data. Since the largest error made using Relation 20" (dynamic limit) to calculate the detachment diameter instead of Relation 20 (general solution) for Ja ≥ $\bar{\mathrm{Ja}}$ is less than 20%, it is simpler to use Relation 20", i.e.,

$$R_{d_2}=c_m\, c_3^{1/3}\left(\frac{a}{g^2}\right)^{1/3}\mathrm{Ja}^{(4/3)m} \qquad (A.5)$$

Thus, we get c_3= 1.228